JMEPEG (2008) 17:20–24
DOI: 10.1007/s11665-007-9164-6
©ASM International
1059-9495/$19.00

Formation of Irregular Nanocrystalline CeO_2 Particles from Acetate-Based Precursor via Spray Pyrolysis

Chin-Yi Chen, Teng-Kuan Tseng, Chien-Yie Tsay, and Chung-Kwei Lin

(Submitted May 15, 2006; in revised form November 13, 2006)

Ultrasonic spray pyrolysis of acetate-based salt precursor with various concentrations is employed to produce nanocrystalline CeO_2 particles in this study. The mean particle size of as-pyrolyzed CeO_2 powders produced from precursor concentrations of 1.0, 0.1, and 0.01 wt.% are 350, 185, and 95 nm, respectively. We found that due to the low solubility of the precursor, the formation of a shell occurs during pyrolysis, leading the CeO_2 particles to be bowl-like in shape with uneven surfaces. Precursor concentrations significantly determine the size of the product particles. The bimodal size distribution of the product particles suggests that both one-particle-per-drop and gas-to-particle conversion mechanisms are active in the process.

Keywords CeO_2, precursor, solubility, spray pyrolysis

1. Introduction

Spray pyrolysis has been widely used to prepare nanocrystalline powders because it is an inexpensive and continuous, ambient pressure process offering numerous possibilities for controlled synthesis of advanced ceramic powders and films (Ref 1). For example, cerium oxide (ceria, CeO_2) has generated considerable interest in its applications to gas sensors (Ref 2), catalytic supports in automotive exhaust system (Ref 3-5), and electrolyte in solid-oxide fuel cell (Ref 6, 7). Generally speaking, fine ceramic powders are highly desirable because they result in high reactivity and high packing density and, thus, enhance the densification of powders with uniform microstructure at low sintering temperature due to their high specific surface area (Ref 6).

Precursor drops undergo three major steps during the process of spray pyrolysis: (1) drop size shrinkage due to evaporation, (2) conversion of precursor into oxides, and (3) solid particle formation. Kodas and Hampden-Smith demonstrated that particle formation may involve two major mechanisms: intraparticle reaction (conventional one-particle-per-drop mechanism) and gas-to-particle conversion (Ref 8). In the one-particle-per-drop mechanism, each droplet is regarded as a micro reactor and converts into one solid particle when it travels through the tubular reactor. In contrast, gas-to-particle conversion occurs when the precursor is volatile and is transported across the particle-gas interface (Ref 8, 9). The vapor of the product materials, after being formed by chemical reaction in the gas phase, may either condense on the particles or nucleate to form new particles. Zhang et al. (Ref 10) demonstrated the influence of zirconium precursor saturation concentrations on zirconia particle morphology in spray pyrolysis using a conventional ultrasonic nebulizer. They also stated that the precipitated salt must not undergo plastic deformation or melting during heating.

The effect of the degree of precursor solution saturation on particle morphology has been investigated by several investigators (Ref 1, 10). In this work, nanocrystalline cerium oxide powder was prepared from the precursor of cerium acetate (CeA, $Ce(C_2H_3O_2)_3{\cdot}1.5H_2O$) with low solution saturation by conventional ultrasonic spray pyrolysis. Precursor drop size was measured precisely to determine the relationships with particle morphology of the resulting CeO_2 product powders and the underlying particle formation mechanisms. A bimodal particle size distribution was found, suggesting that both one-particle-per-drop and gas-to-particle conversion mechanisms were involved in spray pyrolysis. We also found very different particle morphology of CeO_2 produced in this study. Otherwise, precursor does not melt before chemical reaction occurs, resulting in the hollow particles (Ref 11). Subsequently, bowl-like particles with uneven surfaces were formed, indicating formation of nonpermeable plastic shells during cooling.

2. Experimental

2.1 Materials Preparation

The precursor used for generation of CeO_2 particles in this study was cerium acetate (CeA). The chemical formula of CeA is $Ce(C_2H_3O_2)_3{\cdot}1.5H_2O$ (99.9%, Alfa Aesar, A Johnson Matthey Co.). The molecular weight of CeA reported by the manufacturers is 344. The concentration of precursor solutions, CeA in de-ionized water, ranged from 0.01 to 1.0 wt.%.

2.2 Spray Pyrolysis System

A schematic diagram of the spray pyrolysis system is shown in Fig. 1. The precursor droplets were generated by a

Chin-Yi Chen, Chien-Yie Tsay, and **Chung-Kwei Lin**, Department of Materials Science and Engineering, Feng Chia University, Taichung 407, Taiwan, ROC; and **Teng-Kuan Tseng**, Department of Materials Science and Engineering, University of Florida, Gainesville, FL 32611. Contact e-mail: chencyi@fcu.edu.tw.

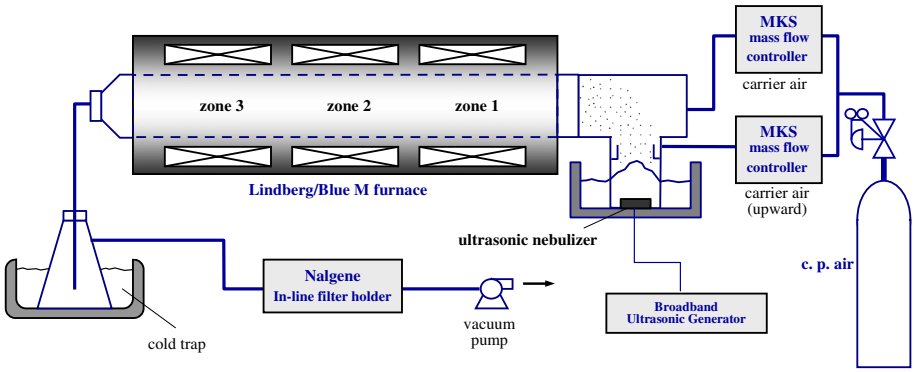

Fig. 1 Schematic diagram of spray pyrolysis system

1.65 MHz ultrasonic transducer. As shown in this figure, the upward airflow first carries the atomized precursor drops into the T-adaptor where additional air is provided through a distributor to carry the precursor drops into the three-zone reactor. The total flow rate of the carrier air maintains at 31 L/min. The temperature set point at zone 2 of the furnace is the reaction temperature and the temperatures of zone 1 and zone 3 are set at 200 °C and 350 °C, respectively. Since the effect of reaction temperature ranging from 650 to 750 °C on particle size and morphology in the rather narrow drop size range employed was found negligible (Ref 12), the reaction temperature used in this study was chosen as 650 °C for CeO_2 formation. Provided with a vacuum pump downstream from the reactor, the carrier air controls the residence time of the precursor drops flowing through the reactor (Ref 12). The residence time in the hot zone with a temperature >550 °C is 3.2 s. The resulting product particles are collected in cold traps and on a polymer filter (0.45 μm pore size, ADVANTEC MFS, Inc., USA) positioned between the cold traps and the vacuum pump.

2.3 Product Characterization

2.3.1 Thermogravimetric Analysis (TGA). Characterization of the precursor was carried out by thermogravimetric analysis (Perkin-Elmer Model TGA-7) under nitrogen flow for removal of product gases. The heating rate was set at 40 °C/min.

2.3.2 Phase Identification of Precursor Pyrolysis Products. The phase identification of product particles was performed by X-ray diffractometry (Philips X'pert PW3040, Philips Co., Netherlands) with CuKα radiation. The phase identification of hydrolyzed CeA was also carried out on the powder precipitated from the CeA aqueous solution at approximately 80 °C.

2.3.3 Microstructure Observation and Determination of Particle Size Distribution. The morphology of spray-pyrolyzed particles was examined using field emission scanning electron microscopy (SEM, Model 1530, Leo, Germany). Finally, the particle size distribution was determined by number counting over 1000 particles from the SEM micrographs.

2.3.4 Measurement of Drop Size Distribution. The drop sizes and size distribution were measured using Malvern Spraytec RTS 5000. The instrument was calibrated using a reticle, Malvern/INSITEC Model (RS-3 and 0.5 μm diameter particles standard. Furthermore, NIST-Traceable Microspheres with diameters ranging from 20 to 900 nm (3000 Series—Polymer Nanosphere^{TM}, Duke Scientific Corp.) were also used.

3. Results and Discussion

In order to determine the relationships of size distribution between precursor drops and resulting particles, the precursor drop size was measured precisely by using a laser light-scattering instrument in this study. Figure 2 shows the size distributions of the precursor drops generated by an ultrasonic nebulizer at 1.65 MHz. It can be noticed that the water and precursor droplets are almost the same in size distribution due to the diluted precursor concentration. They both are uniform with sizes ranging from 4 to 9 μm and peak diameter of about 6 μm. According to the Kelvin equation (Ref 13, 14), the drop size generated by ultrasonic nebulizer depends on the surface tension of the atomized liquid. It implies that the surface tension of precursor solution can be regarded as the same with water when precursor concentration is low (Ref 12).

The TGA weight loss and its differential curve of CeA precursor are shown in Fig. 3. Both the curves (a) and (b) show that CeA underwent three major weight loss mechanisms in the temperature ranges of 200-300 °C, 350-500 °C, and 500-700 °C. Based on the molecular weights of CeA and its decomposition products, the first and the last loss mechanisms were attributable to dehydration and conversion into CeO_2, respectively. The XRD patterns of the particles obtained from spray pyrolysis of CeA with concentration of 1.0 wt.% at 650 °C is shown in Fig. 4. Comparison of this pattern to the standard (Ref 15) leads to identification of the particles obtained from CeA precursor as CeO_2. It can be noticed from the broad diffraction peaks that the grain size of the as-prepared CeO_2 powder after reaction at 650 °C exhibited nanocrystalline structure. Based on the calculation of Scherrer equation, the crystal size of the resulting product powder was estimated to be about 10 nm. Furthermore, the XRD data shown in the inset of Fig. 4 for the precipitates from the hydrolysis of CeA at 80 °C serve to confirm formation of cerium hydroxide (Ref 16). The loss mechanism shown in Fig. 3 for the temperature range of 350-500 °C was attributed to decomposition of CeA to acetic acid and cerium hydroxide. Though not shown here, the melting temperature of acetate precursor was demonstrated in the previous study of Liu and Laine (Ref 17) to be very low

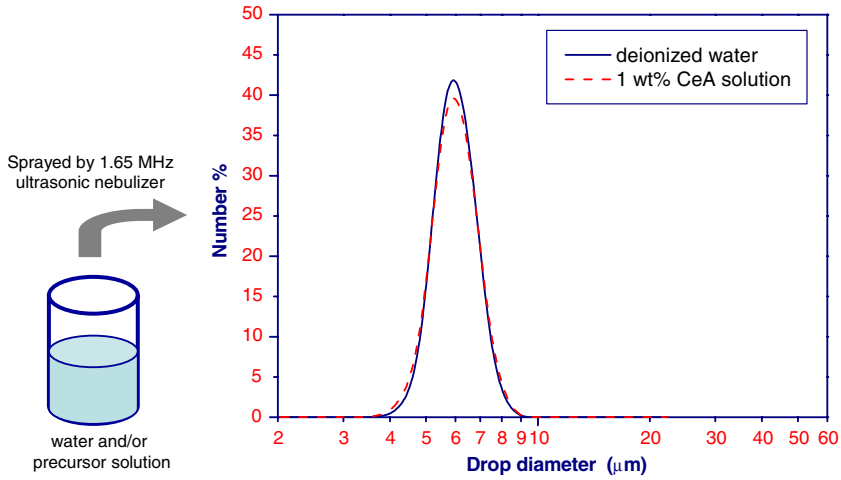

Fig. 2 The size distributions of precursor drops

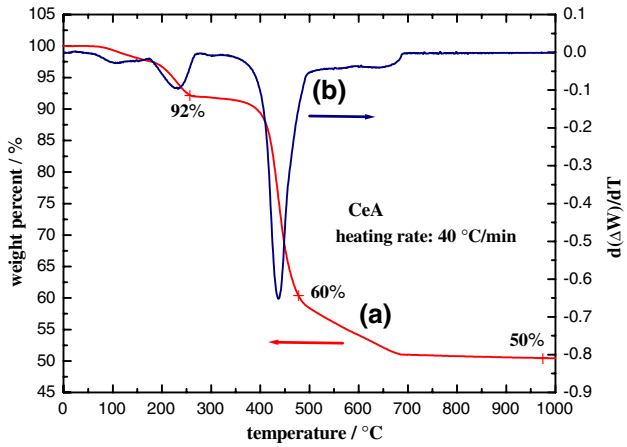

Fig. 3 TGA curve and its weight loss differential curve of precursor CeA

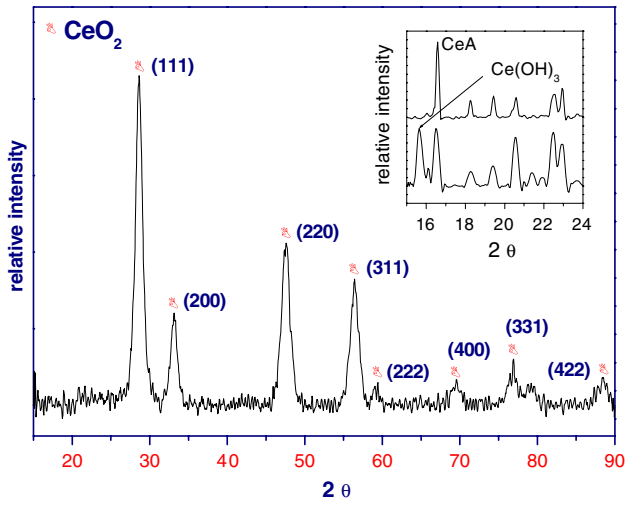

Fig. 4 The XRD patterns of particles obtained from spray-pyrolyzed CeA precursors. The inset shows the XRD patterns of as-received CeA and the precipitates from the hydrolysis of CeA at 80 °C

(~300 °C), suggesting the volatile property of the acetate precursor. Moreover, the rapid heating rate may cause the overheating and enhance the volatility of the precursor during pyrolysis.

Figure 5 shows SEM micrographs of CeO_2 powders obtained from spray pyrolysis of precursor solutions with various CeA concentrations of 0.01, 0.1, and 1.0 wt.%. It can be seen clearly from the morphologies that the CeO_2 particle sizes decrease with decreases in precursor concentration. Figure 6 shows the particle size distribution measured from the micrographs of the spray-pyrolyzed precursor solutions with various CeA concentrations. The mean particle size of CeO_2 powders pyrolyzed from precursor concentrations of 1.0, 0.1, and 0.01 wt.% are 351, 185, and 94 nm, respectively. Moreover, it is interesting to note in Fig. 5 that the CeO_2 particles are bowl-like in shape with uneven surfaces. The particle morphology may be attributed to the effect of precursor solubility that determines how concentrated the precursor solution can be before precursor precipitation occurs (Ref 10).

According to the inference in the case of CeA precursor, as shown in Fig. 7, we schematically diagramed the formation process of irregular CeO_2 particle during spray pyrolysis. The solute precipitates rapidly to form a solid shell within the droplet surface due to its low solubility in water (~260 g/L at room temperature). During the hydrolysis of solute at low temperature (~80 °C), a large amount of solvent evaporates through this permeable shell. With increasing reaction temperature, the cerium hydroxide pyrolyzed into its oxide to form a hollow particle with a denser nanocrystalline shell. As the temperature decreases, the oxide shell with slight deformation ability shrinks and shrivels, resulting in the uneven surface, as shown in Fig. 5. If the deformation is too great, the larger stress may induce the fracture on the surface of particle during shrinkage. It can be noticed from the cracks on some large particles that the particles are hollow, even some of them reveal a bowl-like shape. Moreover, the uniformity of the precipitates in each droplet should influence the shape of particles. It may also cause the particles to be irregular or have uneven surfaces. We believed that the significant irregular formation of CeO_2 particle resulted from larger precursor droplet generated from ultrasonic vibration and the rapid precipitation of solute after supersaturation. It implies that

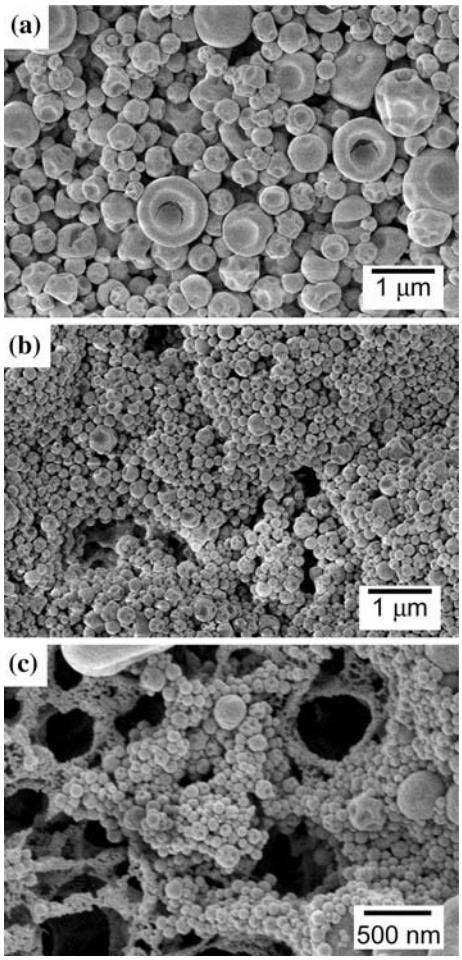

Fig. 5 SEM micrographs of CeO_2 powders obtained from spray pyrolysis of precursor solution with CeA concentration of (a) 1.0, (b) 0.1, and (c) 0.01 wt.%

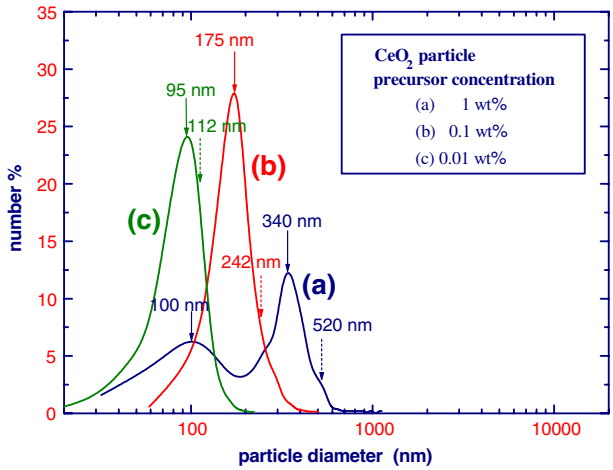

Fig. 6 The size distribution of CeO_2 particles obtained from CeA precursor concentrations of (a) 1 wt.%, (b) 0.1 wt.%, and (c) 0.01 wt.% at reaction temperature of 650 °C

larger CeO_2 particle generated from larger precursor droplet and higher precursor concentration shows to be more irregular in shape after spray pyrolysis.

Additionally, it can be noticed in Fig. 6 that the particle size distribution of CeO_2 particle which pyrolyzed from 1.0 wt.% CeA precursor solution was bimodal at two peak sizes of 340 and 100 nm. The bimodal size distribution suggests that two possible mechanisms occur during the conversion of droplets into solid particles. The larger peak diameter results from the conventional one-particle-per-drop mechanism, while the smaller peak diameter results from the gas-to-particles conversion mechanism. The gas-to-particle conversion occurs when the precursor is volatile, resulting in the vaporized precursor species to form new particles (Ref 8). This may indicate that vaporization of precursor CeA during heating takes place to a considerable degree and some CeO_2 particles are formed via the gas-to-particle conversion mechanism rather than the one-particle-per-drop mechanism. The oxide, subsequently, after being formed by chemical reaction of the precursor in the gas phase, may nucleate to form new small particles. Ultrafine particles resulted from the evaporation of precursor can thus be found in the micrographs of Fig. 5(a).

In the one-particle-per-drop mechanism of spray pyrolysis, each droplet is regarded as a micron reactor converting into solid particle when it travels through the tubular reactor. Based on the conservation of oxide mass, we derived the following equation to calculate the diameter of the particle (d_p) from the precursor drop diameter (d) (Ref 12):

$$d_p = d \cdot \sqrt[3]{\frac{\rho_s \cdot w}{\rho_p}}$$

where w is the precursor concentration in terms of weight fraction of oxide. For example, the concentration of 1 wt.% CeA converts into CeO_2 with a weight loss of 50 wt.%. $w = 0.01 \times (1 - 0.50)$. ρ_s and ρ_p are the densities of the precursor solution (1 g/cm^3) and the resulting CeO_2 particle (7.65 g/cm^3), respectively. Using this equation, particle diameters for the precursor drop diameters ranging from 4 to 9 μm and precursor concentrations of 1.0, 0.1, and 0.01 wt.% were calculated and listed in Table 1. The respective CeO_2 particle diameters calculated from the smallest diameters of precursor drops (4 μm) are 347, 161, and 74 nm for the precursor concentrations of 1.0, 0.1, and 0.01 wt.%, respectively. It is noticed that the measured larger peak diameters (351, 185, and 94 nm for precursor concentrations of 1.0, 0.1, and 0.01 wt.%, respectively) are similar to the sizes predicted for 4 μm diameter drops. We also indicated the predicted particle size for the peak diameter (6 μm) of drop size by dotted-line arrows in Fig. 6 (520, 242, and 112 nm for precursor concentrations of 1.0, 0.1, and 0.01 wt.%, respectively). The size distributions are still significantly smaller than the sizes predicted for the peak diameter of the precursor drops, shown in Table 1 and Fig. 6. It can also be noticed that the bimodal size distribution was not observed for the particle obtained from the precursor concentrations of 0.1 and 0.01 wt.%, curves (b) and (c) in Fig. 6. Because the concentration of precursor solution is relatively low, the effect of the concentration on the size of the particles generated from gas phase thus tended to be negligible. Single peak diameters may result from the similar size distribution between the particles generated from gas-to-particle conversion and one-particle-per-drop mechanisms. Furthermore, the formation of irregular CeO_2 particles shows to be less significant when precursor concentration is low.

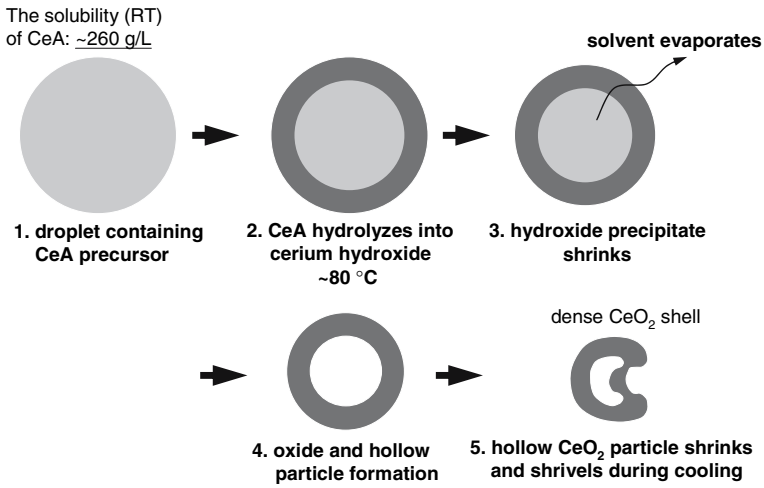

Fig. 7 Schematic representation illustrating the formation of irregular CeO_2 particles during elevating temperature in spray pyrolysis

Table 1 The particle size predicted by the one-particle-per-drop mechanism

	CeA concentration, wt.%		
	1.0	0.1	0.01
Precursor drop size, μm	Predicted product particle size, nm		
4	347	161	74
6 (peak)	520	242	112
9	781	362	168
Measured mean particle size	351	185	94

The precursor solution concentrations involved are 1.0, 0.1, and 0.01 wt.%, respectively. The measured mean sizes are also listed

4. Conclusions

Nanocrystalline CeO_2 particles were prepared from acetate-based precursor using ultrasonic spray pyrolysis. We inferred that the low solubility of CeA precursor resulted in the formation of hydroxide shell and subsequently pyrolyzed into CeO_2 particles at reaction temperature. The resulting CeO_2 particles shrink and shrivel to be bowl-like in shape with uneven surfaces during cooling. Larger CeO_2 particle generated from larger precursor droplet and higher precursor concentration reveals to be more irregular in shape after spray pyrolysis. By precisely measuring the precursor drop size, we show that the gas-to-particle conversion mechanism is also involved in spray pyrolysis, resulting in particle sizes much smaller than those predicted by the one-particle-per-drop mechanism.

Acknowledgment

This research was partially sponsored by the National Science Council, the Republic of China, under the Grant No. NSC93-2216-E-035-026.

Reference

1. G.L. Messing, S.C. Zhang, and G.V. Jayanthi, Ceramic Powder Synthesis by Spray-Pyrolysis, *J. Am. Ceram. Soc.*, 1993, **76**(11), p 2707–2726
2. H.-J. Beie and A. Gnörich, Oxygen Gas Sensors Based on CeO_2 Thick and Thin-Films, *Sensor. Actuat. B*, 1991, **4**, p 393–399
3. M. Ogita, K. Higo, Y. Nakanishi, and Y. Hatanaka, Ga_2O_3 Thin Film for Oxygen Sensor at High Temperature, *Appl. Surf. Sci.*, 2001, **175**, p 721–725
4. H. Xu, L. Gao, H. Gu, J. Guo, and D. Yan, Synthesis of Solid, Spherical CeO_2 Particles Prepared by the Spray Hydrolysis Reaction Method, *J. Am. Ceram. Soc.*, 2002, **85**(1), p 139–144
5. T.C. Rojas and M. Ocaña, Uniform Nanoparticles of Pr(III)/Ceria Solid Solutions Prepared by Homogeneous Precipitation, *Scripta Mater.*, 2002, **46**(9), p 655–660
6. N.Q. Minh, Ceramic Fuel-Cells, *J. Am. Ceram. Soc.*, 1993, **76**(3), p 563–588
7. R.N. Blumenthal, F.S. Brugner, and J.E. Garnier, The Electrical Conductivity of CaO-Doped Nonstoichiometric Cerium Dioxide from 700 to 1500 °C, *J. Electrochem. Soc.*, 1973, **120**(9), p 1230–1237
8. T.T. Kodas and M.J. Hampden-Smith, *Aerosol Processing of Materials*. Wiley-Vch, New York, 1999, p 421
9. A.S. Gurav, T.T. Kodas, J. Joutsensaari, E.I. Kauppinen, and R. Zilliacus, Gas-Phase Particle-Size Distributions and Lead Loss During Spray-Pyrolysis of (Bi,Pb)-Sr-Ca-Cu-O, *J. Mater. Res.*, 1995, **10**(7), p 1644–1652
10. S.-C. Zhang, G.L. Messing, and M. Borden, Synthesis of Solid, Spherical Zirconia Particles by Spray Pyrolysis, *J. Am. Ceram. Soc.*, 1990, **73**(1), p 61–67
11. S. Jain, D.J. Skamser, and T. Kodas, Morphology of Single-Component Particles Produced by Spray Pyrolysis, *Aerosol Sci. Technol.*, 1997, **27**(5), p 575–590
12. Y.L. Song, S.C. Tsai, C.Y. Chen, T.K. Tseng, C.S. Tsai, J.W. Chen, and Y.D. Yao, Ultrasonic Spray Pyrolysis for Synthesis of Spherical Zirconia Particles, *J. Am. Ceram. Soc.*, 2004, **87**(10), p 1864–1871
13. R.J. Lang, Ultrasonic Atomization of Liquids, *J. Acoust. Soc.*, 1962, **34**(1), p 6–8
14. F. Barreras, H. Amaveda, and A. Lozano, Transient High-Frequency Ultrasonic Water Atomization, *Exp. Fluids*, 2002, **33**(3), p 405–413
15. JCPDS (Joint Committee on Powder Diffraction Standards) Card for X-ray Diffraction 01-0800
16. JCPDS Card for X-ray Diffraction 74-0665
17. Y. Liu and R.M. Laine, Spinel Fibers from Carboxylate Precursor, *J. Eur. Ceram. Soc.*, 1999, **19**(11), p 1949–1959